Theoretical and Applied Fracture Mechanics 131 (2024) 104422

Contents lists available at ScienceDirect

Theoretical and Applied Fracture Mechanics

journal homepage: www.elsevier.com/locate/tafmec

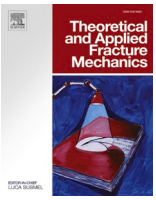

Effects and recommendations of crack tip modelling on compliance solutions

L.G.F. Andrade [a,b,*], M. Mattar Neto [a,b], G.H.B. Donato [a]

[a] Centro Universitário FEI, São Bernardo do Campo, Brazil
[b] Instituto de Pesquisas Energéticas e Nucleares, IPEN–CNEN/SP, São Paulo, Brazil

ARTICLE INFO

Keywords:
Elastic unloading compliance
Crack tip
Blunt mesh
Sharp mesh

ABSTRACT

Elastic unloading compliance is a common technique to determine instantaneous crack size in fracture mechanics properties such as resistance curves (*R-curves*) and fatigue crack growth. This technique uses a polynomial, developed using finite elements models, to correlate compliance with crack depth. In these models, crack tip is usually modeled with a blunt mesh (with a crack tip radius ρ) or a sharp mesh (with element size in the width direction l), and neither are standardized in the literature. This paper shows that both affect compliance, therefore potentially impacting results of fracture mechanics properties acquired from simulations. This paper focuses on how those parameters affects compliance in *SE(B)* models. Finally, a parameter φ that normalizes ρ or l with the width was developed and recommended values based on compliance convergence are suggested. Controlling φ may help to ensure reliable results in fracture mechanics models where compliance needs to be determined.

Nomenclature

Latin

a	Crack depth (mm)
a/W	Relative crack depth (*mm/mm*)
ASTM	American Society for Testing and Materials
B	Model thickness (*mm*)
BM	Crack tip blunt mesh
C	Compliance (*mm/N*)
C_0	Reference compliance (*mm/N*)
C_{DELTA}	Compliance variation (%)
CMOD	Crack Mouth Opening Displacement
da/dN	Fatigue crack growth rate
E	Elastic modulus (*GPa*)
EUC	Elastic Unloading Compliance
FE	Finite Elements
J	*J* integral. Non-linear energy release rate (J/mm^2)
K	Stress intensity factor ($MPa.m^{0.5}$)
l	Element size in the width direction crack tip in a sharp mesh
P	Load (*N*)
R^2	Coefficient of determination
SE(B)	Single-edge-notched under bending specimen
SM	Crack tip sharp mesh
V	displacement (*mm*)
W	Model width (*mm*)

Greek

(*continued on next column*)

(*continued*)

Nomenclature

Latin

ν	Poisson's ratio
ρ	Crack tip radius in a blunt mesh
σ_0	Yield strength (*MPa*)
φ	Correlation between crack tip radius ρ or element size l with the width *W*

1. Introduction

Elastic unloading compliance (*EUC*) is a common technique to determine the instantaneous crack size during resistance curve (*J-R*) and fatigue crack growth tests (*da/dN vs.* ΔK) [1–3]. Clarke et al., were among the first to use *EUC* to determine the resistance curve of a material using a single specimen [4]. This technique is performed by correlating the specimen (or model) compliance with the instantaneous crack size, usually with a fifth order polynomial. The procedure to develop this polynomial is described in detail in the article of Moreira [5] and includes the measurement of the compliance of typical linear elastic *FE* models of real specimens. However, several phenomena can affect compliance. Moreira addressed the effects of side-grooves and

* Corresponding author at: Humberto de Alencar Castelo Branco Avenue, 3972-B - Assunção, São Bernardo do Campo, SP 09850-901, Brazil.
E-mail address: leonardogfa@gmail.com (L.G.F. Andrade).

https://doi.org/10.1016/j.tafmec.2024.104422
Received 24 November 2023; Received in revised form 6 April 2024; Accepted 7 April 2024
Available online 10 April 2024

thickness and other researchers have addressed plasticity [6,7], tunneling [8–12], and specimen rotation [13,14].

Regarding to the crack tip modelling, it is now shown in the literature how it may affect the *EUC* technique. Additionally, the literature does not show consensus on how this region should be modelled, and two main geometries are adopted, being the blunt mesh (*BM*) or a sharp mesh (*SM*) with proper boundary conditions to represent the crack (Fig. 2). It is not clear how the crack tip radius in a blunt mesh or the dimension of element size in the direction of the width in a sharp mesh affects compliance of the models, and there is no reference in the previously mentioned *ASTM* standards on how the compliance solutions were obtained via finite elements simulations regarding to the crack tip modelling [1,2].

Several studies can be mentioned to exemplify the diversity of modelling approaches. For sharp meshes, the element size l near the crack tip can be seen as *1/3000 W* (for *1 T* models, $l = 0.017$ *mm*) [8], collapsed into a straight line [9], *0.001 W* (for *1 T* models, $l = 0.051$ *mm*) [12] among others. For blunt meshes, the crack tip radius ρ is seen with a broader variance. Values of *0.0025 mm* [5,9,15], *0.05 mm* [10,11], *0.075 mm* [6], and $\rho/b = 0.00015$ (for $a/W = 0.5$, $\rho = 0.0039$ *mm*) [14] can be found in the literature.

References of how the crack tip should be modelled are scarce. Graba and Gałkiewicz conducted a study on how the crack tip modelling affect the near crack tip stress fields [16]. This paper concludes that, for a blunt mesh style, the crack tip radius should be between 10^{-3} to 10^{-4} *mm* for the accurate determination of stresses measured at a distance below J/σ_0. When such values are not of a concern, no recommendation of the crack tip modelling is given [16].

The present shows that compliance is impacted by the crack tip radius or the near tip element size and aims to evaluate such effects to support future researchers on the topic to properly model this mesh region.

2. Test methodology

2.1. Geometry

Since the objective of this paper is isolate the impact of crack tip modelling on compliance, it was decided to study a single specimen geometry. For this, *SE(B)* geometry (Fig. 1) was adopted. *1 T* proportions ($B = 25.4$ *mm*, $W/B = 2$) were chosen as a reference, with relative crack depth values of *0.1*, *0.3*, *0.5,* and *0.7*. In addition, to properly evaluate the impact of the width on the results, *0.5 T* ($B = 12.7$ *mm*, $W/B = 2$) and *2 T* ($B = 50.8$ *mm*, $W/B = 2$) were also incorporated in the study with a relative crack depth value of *0.5*.

Initially, *BM* meshes were used with crack tip radiuses ρ of *1*, *0.5*, *0.05*, *0.005,* and *0.0005 mm* each for all conditions. Additionally, two models with *1 T* dimensions with a reduced thickness of $B = 2$ *mm* were also incorporated in the analysis matrix to evaluate the impact of thickness, both on plane stress (unrestricted z-axis node displacement) and plane strain (restricted z-axis node displacement) dominated models. The analysis matrix for *BM* is shown below in Table 1, with a total of *40 FE* models.

SM models were also incorporated, with element sizes in the width directions l of *1*, *0.5*, *0.05*, *0.005,* and *0.0005 mm*. Reduced thickness was not studied with *SM*. Not all conditions were simulated for *SM* because results followed a trend similar to *BM*. The analysis matrix for *SM* is shown below in Table 2, where X represents all values of l, and X* represents $l = 1$ and *0.0005 mm* only.

Schematics of both crack tip modelling approaches, *BM* and *SM*, are shown in Fig. 2.

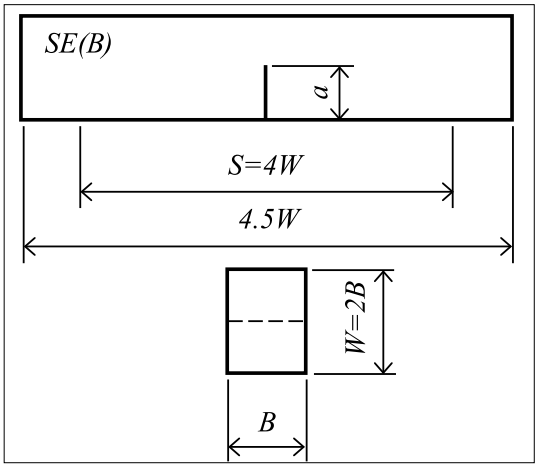

Fig. 1. Schematics of the SE(B) specimen.

3. Materials

To ensure that material choice would not impact the results with effects such as plasticity, a linear elastic material was used. Following Hooke's Law, $E = 206$ *GPa* and $\nu = 0.3$ is enough to represent high strength steel alloys under linear elastic regimen.

4. *FE* models

In accordance with the available literature [8–15], highly refined 3D models were used in this paper. The software Dassault Systèmes Abaqus 2020® [17] was used in this paper. All the major characteristics of the models are listed below:

- One quarter of the SE(B) specimen was modeled to save computational time. Usual double symmetry boundary conditions are applied (z-direction displacement restricted on the xy plane for the central nodes of the model and y displacement restricted on the xz plane for the remaining ligament).
- Ten elements were used to describe the half thicknesses of *0.5 T* and *1 T* and twenty elements for *2 T*. Element size for the thickness followed a linear progression, with the ratio between the surface and the central element being 0.1.
- Total number of nodes and elements ranges from 17 thousand in the smallest model with coarsest mesh (*0.5 T*, $\rho = 1$ *mm*) to 130 thousand in the largest and most refined mesh (*2 T*, $\rho = 0.0005$ *mm*). A model example is shown in Fig. 3.
- Eight node hexahedral linear integration elements were used (Abaqus® *C3D8*). In the analyzed conditions, no relevant differences were detected when comparing results with *20*-node quadratic integration elements (Abaqus® *C3D8*). A comparison is shown is Fig. 5. The authors acknowledge that for more complex simulations that may involve plasticity and/or higher loading and displacement, the latter element option should be prioritized.
- Loading was applied to the models as displacement at the central nodes of the crack plane (x direction only), representing the roller of the three-point-bending device. A total of *100* increments of *0.002 mm* were added at each step of the simulation totalizing *0.2 mm* of displacement, and in the next simulation phase the model is completely unloaded. Similarly to the loading, the specimen was

Table 1
Analysis matrix for models with blunt mesh crack tip.

***BM* MODELS**	***a/W***			
	0.1	**0.3**	**0.5**	**0.7**
0.5 T			X	
1 T	X	X	X	X
1 T B = 2 mm			X	
2 T			X	

Table 2
Analysis matrix for models with sharp mesh crack tip.

SM MODELS	*a/W*			
	0.1	**0.3**	**0.5**	**0.7**
0.5 T			X	
1 T	X*		X	X*
2 T			X	

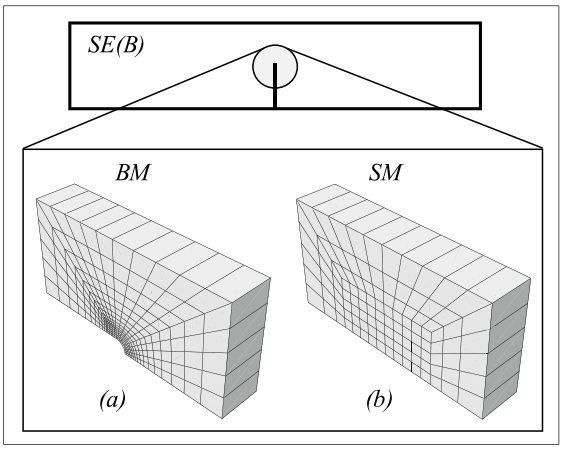

Fig. 2. Examples of (a) BM and (b) SM crack tip designs (symmetric).

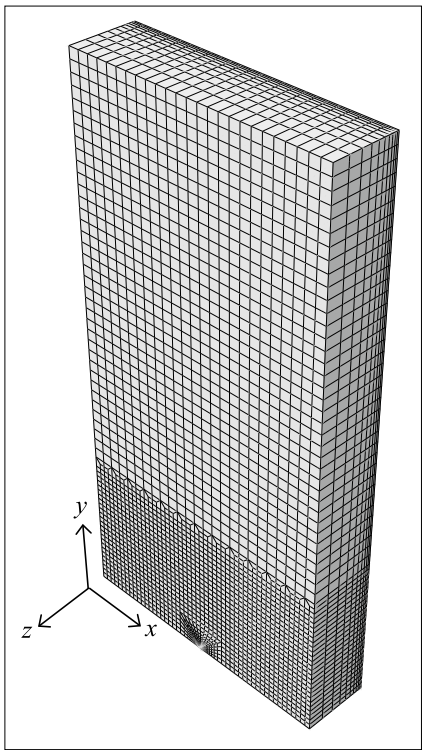

Fig. 3. Example of a SE(B) model.

supported by applied displacement restriction (x direction only) to the nodes that represent the bottom roller of the three-point-bending device. It is worth observing that for nonlinear simulations with greater levels of loading, detailed roller contact modelling is desired and should enhance the representativeness of the SE(B) simulations [10].

- Load P is registered at the nodes representing the top loading pin. Values of multiple nodes are added and multiplied by a factor of four to account for double symmetry. Displacement V is registered as an average of the vertical displacement of the nodes in the leftmost line of the crack plane that represents the crack mouth opening displacement (*CMOD*). Values are averaged and then multiplied by a factor of two to account for symmetry.
- The relationship V/P is determined for all simulation steps. Compliance is registered only for the unloading phase. Top and bottom 10 % values are discarded for calculations to ensure that the relationship is linear [1,2].

5. Results

The main results are shown as compliance delta (C_{DELTA}, eq.1) function of crack tip radius (ρ) for *BM* or element size (l) for *SM*. C_{DELTA} is a parameter that shows the percentual evolution of compliance C in relation to a reference measure C_0, effectively representing a convergence of the simulations. Since chosen values of ρ and l represent various scales of magnitude, results are displayed in a logarithm scale for better understanding. Compliance for the smallest crack tip radius or crack tip element size ($\rho = l = 0.0005\ mm$) is adopted as a reference C_0 for C_{DELTA} calculations since these values should be more representative of the sharpness of a real crack. In the graphics, markers represent results of *FE* analysis and are connected via trend lines. For the first result, an additional graph (Fig. 5) is shown comparing C_{DELTA} for the *SE(B)*, $a/W = 0{,}5$, *1 T* modelled with *C3D8* and *C3D20* elements. The trend is captured by both models, and all remaining simulations were conducted with *C3D8*. The main objective is to verify the convergence of the results and both alternatives should provide similar results.

$$C_{DELTA} = \frac{(C\text{-}C_0)}{C_0} 100 \quad (1)$$

Results are divided into three sections – *BM*, *SM,* and comparison.

5.1. Section 1 – Blunt mesh

Results for the *SE(B) 1 T* using *BM* mesh are shown in Table 3 for compliance C (for convenience, displayed as 10^{-6} *mm/N*), Table 4 for compliance delta, and Fig. 4 for compliance delta versus crack tip radius.

It is shown that for all relative crack depths, when a crack tip radius above *0.05 mm* is used the impact on compliance is greater than *0.5 %* and may be relevant. To verify if the thickness has any impact on the results above, results for a reduced thickness *SE(B)*, $a/W = 0.5$, *1 T* $B = 2\ mm$ are shown below in Tables 5–6 and Fig. 6. Such models differ from the detailed in the previous section only for the thickness modelling. Only one element layer of 1 mm width is considered. Symmetry is considered at the *xy* plane, effectively representing $B = 2\ mm$. For plane strain, additional *z*-direction restriction is applied on the opposite side of the model.

Comparing data from Table 4, $a/W = 0.5$ and Table 6, there are very few differences. Maximum errors ($\rho = 1\ mm$) for plane stress, plane strain (Table 6), and full 3D (Table 4) are respectively *3.044 %*, *2.951 %,* and *3.209 %*. Since C_{DELTA} is on the same scale of magnitude and the variation between the three values is within *0.3 %*, this points to no

Table 3
Compliance for SE(B), all a/W,1T, BM mesh.

C $[10^{-6}$ *mm/N]*	*a/W*			
ρ [mm]	**0.1**	**0.3**	**0.5**	**0.7**
1	0.630	2.419	6.881	24.891
0.5	0.615	2.387	6.774	24.311
0.05	0.603	2.357	6.677	23.792
0.005	0.602	2.355	6.668	23.740
0.0005	0.602	2.354	6.667	23.736

Table 4
C_{DELTA} for SE(B), all a/W, 1 T, BM mesh.

C_{DELTA}	a/W			
ρ [mm]	0.1	0.3	0.5	0.7
1	4.535	2.763	3.209	4.864
0.5	2.189	1.372	1.604	2.423
0.05	0.190	0.131	0.156	0.233
0.005	0.007	0.009	0.011	0.017
0.0005	0	0	0	0

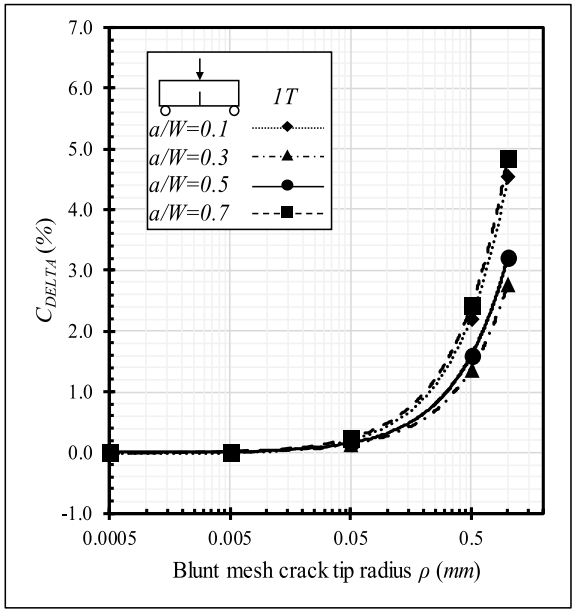

Fig. 4. C_{DELTA} versus ρ for SE(B), all a/W, 1 T, BM mesh.

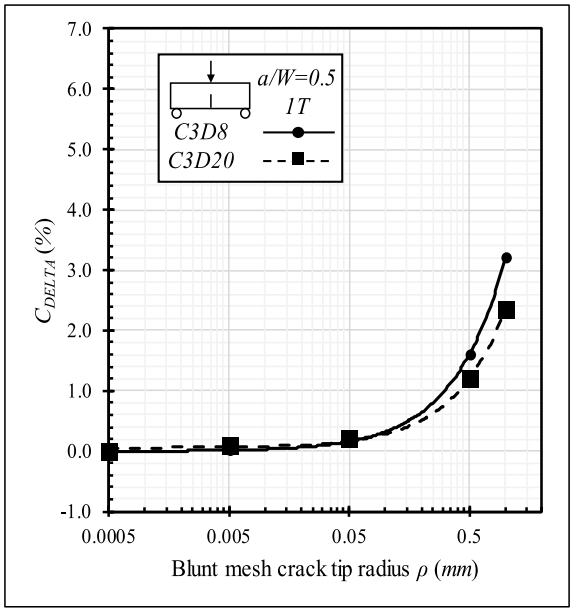

Fig. 5. C_{DELTA} versus ρ comparison between C3D8 and C3D20 elements for SE (B), a/W = 0,5, 1 T, BM mesh.

expressible impact of the thickness on compliance results. This is in accordance with the literature [5].

The impact of the width on the crack tip modelling was addressed

Table 5
Compliance for SE(B), a/W = 0.5, 1 T B = 2 mm in plane stress and plane strain.

C [10^{-6} mm/N]	Stress state	
ρ [mm]	Plane stress	Plane strain
1	88.782	80.850
0.5	87.495	79.689
0.05	86.298	78.646
0.005	86.169	78.541
0.0005	86.159	78.533

Table 6
C_{DELTA} for SE(B), a/W = 0.5, 1 T B = 2 mm in plane stress and plane strain.

C_{DELTA}	Stress state	
ρ [mm]	Plane stress	Plane strain
1	3.044	2.951
0.5	1.550	1.473
0.05	0.161	0.144
0.005	0.011	0.011
0.0005	0	0

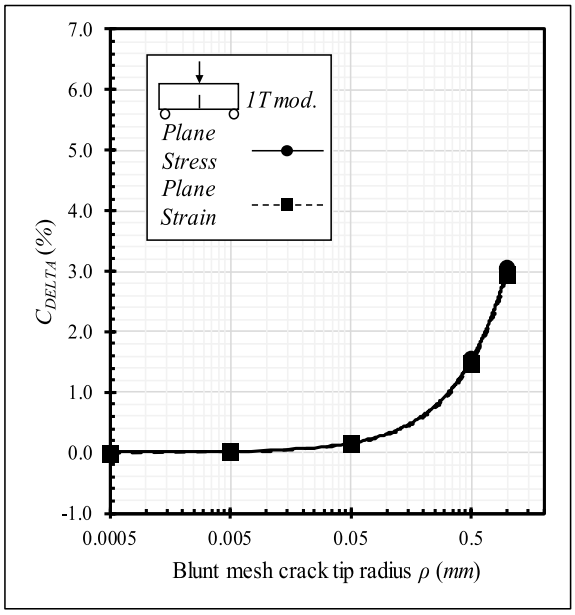

Fig. 6. C_{DELTA} versus ρ for SE(B), a/W = 0.5, 1 T B = 2 mm in plane stress and plane strain.

next. This was achieved with *0.5 T* and *2 T* models. Since no impact of thickness was found, the distinct thickness of the model proportions should not impact the results. Only the $a/W = 0.5$ condition was studied, since the behavior is similar for the other relative crack depths described in this paper (Fig. 4). Comparisons between the *SE(B)*, $a/W = 0.5$ *0.5 T*,

Table 7
Compliance for SE(B), a/W = 0.5,0.5 T, 1 T, and 2 T, BM mesh.

C [10^{-6} mm/N]	Proportion		
ρ [mm]	0.5 T	1 T	2 T
1	14.152	6.881	3.391
0.5	13.731	6.774	3.364
0.05	13.343	6.677	3.340
0.005	13.304	6.668	3.337
0.0005	13.301	6.667	3.337

1 T, and *2 T* using *BM* are shown in Tables 7–8 and Fig. 7.

The behavior of the three proportions studied is very similar. The major difference is the intensity of the C_{DELTA} increases with crack tip radius, which is higher for *0.5 T* and lower for *2 T*. Further observation leads to normalization with the width. A parameter φ is now defined as the crack tip radius normalized by the width, as shown in eq.2. A factor of 10^3 was used for convenience. Results shown in Fig. 7 are shown again in Fig. 8 as C_{DELTA} versus φ. Such parameter allows a convergence analysis in a precise way.

$$\varphi = 10^3 \rho / W \quad (2)$$

5.2. Section 2 – Sharp mesh

Results for the *SE(B) 1 T* using *SM* mesh are shown in Table 9 for compliance, Table 10 for compliance delta, and Fig. 9 for compliance delta versus crack tip element size. The $a/W = 0.3$ condition is not displayed here and $a/W = 0.1$ and *0.7* have only extreme values of l (*1* and *0.0005 mm*).

Comparing Tables 3 and 9, the compliance results for $\rho = l = 0.0005$ *mm* are the same. This indicates that the methodology of adopting the reference at these values is reasonable for the calculation of C_{DELTA}.

Negative C_{DELTA} is observed with *SM* modelling. This implies that the model becomes more rigid with a higher element size. This can be justified since larger *C3D8* elements should be unable to properly describe the crack tip blunting. In addition, C_{DELTA} is less sensitive to l than to ρ. Comparing Tables 4 and 10, maximum absolute errors for $a/W = 0.5$ are *3.209 %* and *1.682 %*.

The same comparison shown in Tables 7–8 and Fig. 7 is now replicated using a sharp mesh crack tip. Comparisons between the *SE(B)*, $a/W = 0.5$ *0.5 T, 1 T,* and *2 T* using *SM* are shown in Tables 11–12 and Fig. 10.

Finally, Fig. 11 shows φ is a function of the element size l, as shown in Eq. (3).

$$\varphi = 10^3 l / W \quad (3)$$

5.3. Section 3 – Comparison

A very strong correlation between the normalization of compliance (C_{DELTA}) and the normalization of the crack tip radius or element size (ρ, l) is observed in Figs. 8 and 11, with a linear relationship. Considering data from all model proportions for *BM* and *SM* separately, Fig. 12 shows C_{DELTA} function of φ for both cases. Here, *x*-axis is in linear scale. Linear equations for the trend line alongside correlation R^2 values are also displayed.

It is important to emphasize that the results below are for *SE(B)*, $a/W = 0.5$ only. On the other hand, even though C_{DELTA} may vary slightly between other crack depths (Table 4, Fig. 4), the scale of magnitude does not change. In addition, crack tip modelling is usually constant for all models in a study. Knowing that, Fig. 12 should be adequate for all *SE (B)*.

Tables 13–14 show values for φ, ρ, and l for various C_{DELTA} values. Higher values of ρ and l might be necessary due to computation limitations, analysis involving plasticity, and other study dependent factors. Researchers should exercise caution and account for compliance errors

Table 8
C_{DELTA} for SE(B), a/W = 0.5,0.5 T, 1 T, and 2 T, BM mesh.

C_{DELTA}	Proportion		
ρ [mm]	0.5 T	1 T	2 T
1	6.397	3.209	1.600
0.5	3.231	1.604	0.793
0.05	0.317	0.156	0.077
0.005	0.023	0.011	0.006
0.0005	0	0	0

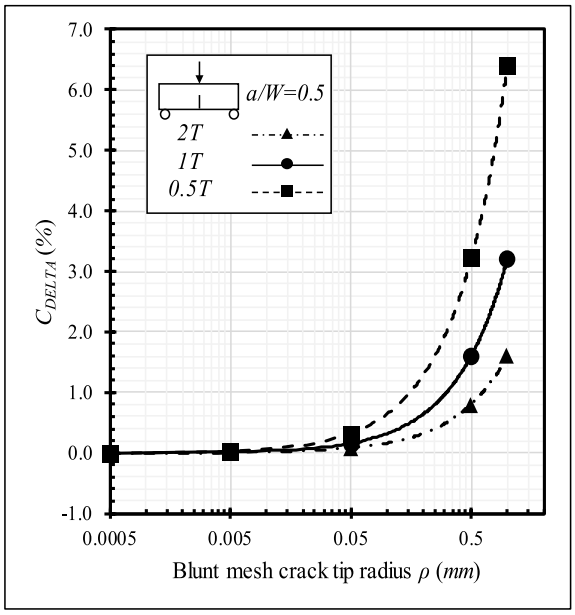

Fig. 7. C_{DELTA} versus ρ for SE(B), a/W = 0.5,0.5 T, 1 T, and 2 T, BM mesh.

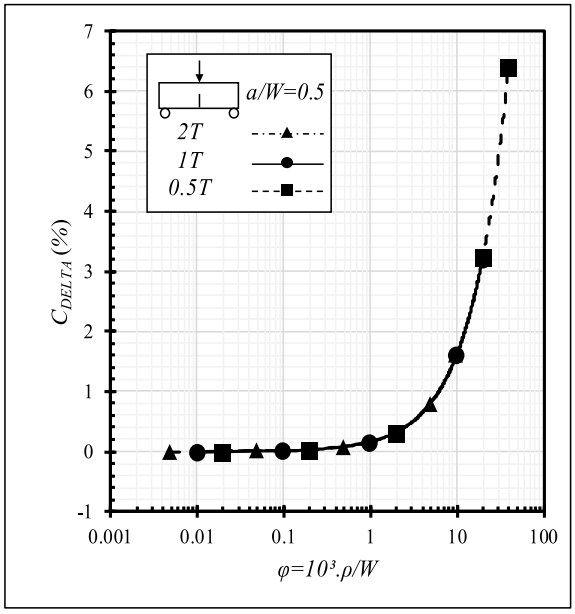

Fig. 8. C_{DELTA} versus φ for SE(B), a/W = 0.5,0.5 T, 1 T, and 2 T, BM mesh.

Table 9
Compliance for SE(B), all a/W, 1 T, SM mesh.

C [10^{-6} mm/N]	a/W			
l [mm]	0.1	0.3	0.5	0.7
1	0.585		6.555	23.182
0.5			6.610	
0.05			6.661	
0.005			6.666	
0.0005	0.602		6.667	23.735

Table 10
C_{DELTA} for SE(B), all a/W, 1 T, SM mesh.

C_{DELTA}	a/W			
l[mm]	0.1	0.3	0.5	0.7
1	−2.866		−1.682	−2.333
0.5			−0.856	
0.05			−0.086	
0.005			−0.007	
0.0005	0		0	0

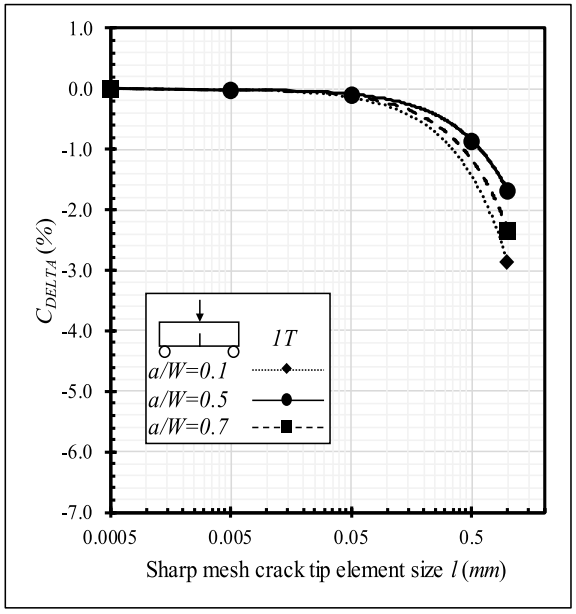

Fig. 9. C_{DELTA} versus l for SE(B), all a/W, 1 T, SM mesh.

Table 11
Compliance for SE(B), a/W = 0.5,0.5 T, 1 T, and 2 T, SM mesh.

C [10^{-6} mm/N]	Proportion		
l[mm]	0.5 T	1 T	2 T
1	12.862	6.555	3.308
0.5	13.075	6.610	3.322
0.05	13.277	6.661	3.335
0.005	13.298	6.666	3.337
0.0005	13.300	6.667	3.337

Table 12
C_{DELTA} for SE(B), a/W = 0.5,0.5 T, 1 T, and 2 T, SM mesh.

C_{DELTA}	Proportion		
l[mm]	0.5 T	1 T	2 T
1	−3.289	−1.682	−0.852
0.5	−1.691	−0.856	−0.431
0.05	−0.172	−0.086	−0.043
0.005	−0.015	−0.007	−0.004
0.0005	0	0	0

that might occur from using higher φ values in their analysis.

6. Conclusions

- Absolute errors in compliance increase with higher values of ρ and l, demonstrating that the crack behavior is less represented in models with higher values (Figs. 4–11).

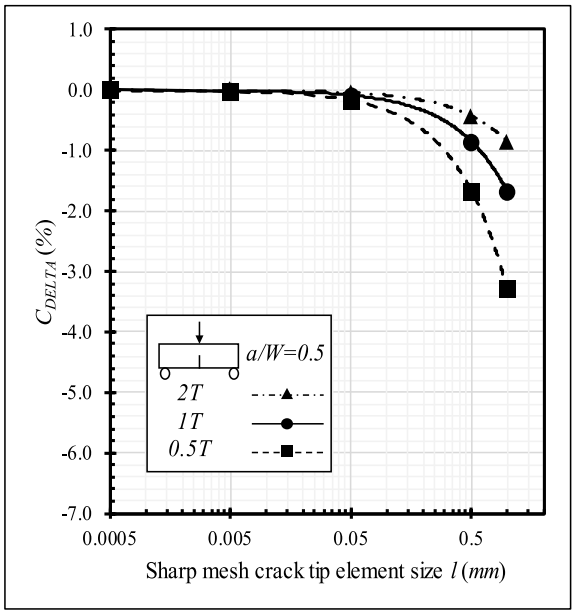

Fig. 10. C_{DELTA} versus ρ for SE(B), a/W = 0.5,0.5 T, 1 T, and 2 T, SM mesh.

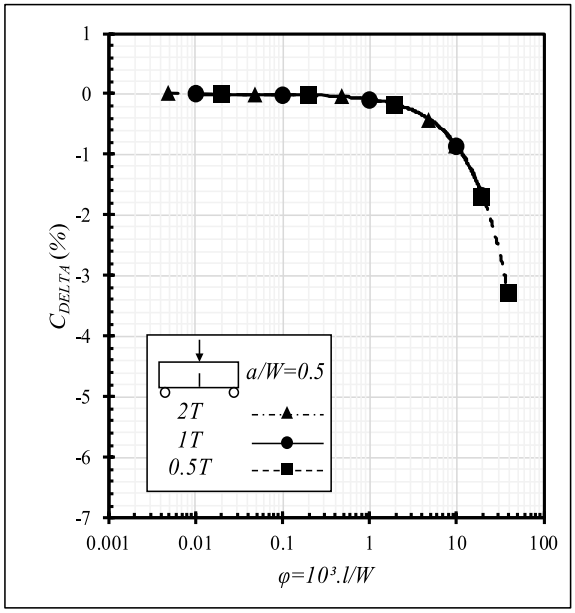

Fig. 11. C_{DELTA} versus φ for SE(B), a/W = 0.5,0.5 T, 1 T, and 2 T, SM mesh.

- No impact of the thickness was found on the relationship between compliance and the increasingly crack tip radius (Tables 4–6).
- Comparing *BM* and *SM* models shows that compliance results are the same for $\rho = l = 0.0005$ *mm*, demonstrating that the methodology of adopting the reference at these values for the calculation of C_{DELTA} is reasonable (Tables 3 and 9).
- Comparison of results for *SE(B)*, $a/W = 0.5$, *0.5 T*, *1 T*, and *2 T* showed that the impact in compliance of crack tip radius and crack tip element size is influenced by the width *W* (Figs. 7 and 10).
- A parameter φ (eq.2–3) was created, and the recommended values are $\varphi \leq 1.5$ (*BM*, Table 13) and $\varphi \leq 2.8$ (*SM*, Table 14), which should yield absolute errors below *0.25 %* in all cases for hexahedral linear integration element models (Fig. 12).
- If higher φ are needed on simulations, caution should be exercised and a sensitivity analysis of ρ or l is recommended.

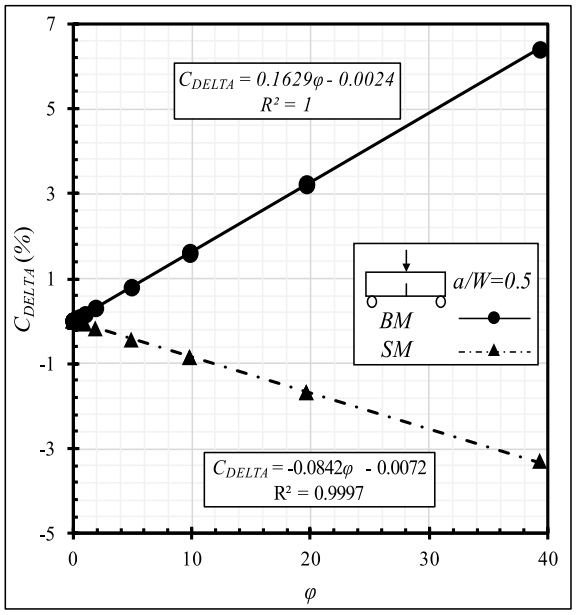

Fig. 12. C_{DELTA} versus φ linear relationship for BM and SM meshes (SE(B), a/W = 0.5).

Table 13
Values for φ and ρ for various C_{DELTA} targets (SE(B), a/W = 0.5).

C_{DELTA} magnitude		*0.5 T*	*1 T*	*2 T*
	φ	*ρ [mm]*	*ρ [mm]*	*ρ [mm]*
0.25	1.52	0.038	0.077	0.154
0.50	3.05	0.077	0.155	0.310
1	6.12	0.156	0.311	0.622
2	12.26	0.311	0.623	1.246

Table 14
Values for φ and l for various C_{DELTA} targets (SE(B), a/W = 0.5).

C_{DELTA} magnitude		*0.5 T*	*1 T*	*2 T*
	φ	*L [mm]*	*L [mm]*	*L [mm]*
−0.25	2.88	0.073	0.146	0.293
−0.50	5.85	0.149	0.297	0.594
−1	11.79	0.299	0.599	1.198
−2	23.67	0.601	1.202	2.405

7. Suggestions for future work

The authors suggest that research on how the parameter φ affects obtained values of crack driving forces (stress intensity factor, CTOD, *J* integral and resistance curves) from simulations should be conducted to complement this paper.

CRediT authorship contribution statement

L.G.F. Andrade: Writing – review & editing, Writing – original draft, Methodology, Data curation, Conceptualization. **M. Mattar Neto:** Writing – review & editing, Writing – original draft, Supervision. **G.H.B. Donato:** Writing – review & editing, Supervision, Formal analysis, Conceptualization.

Declaration of competing interest

The authors declare that they have no known competing financial interests or personal relationships that could have appeared to influence the work reported in this paper.

Data availability

Data will be made available on request.

Acknowledgements

The authors would like to acknowledge CNPQ (grant 486176/2013-4), CAPES and FEI University for all the support given to complete this paper.

References

[1] American Society for Testing and Materials, ASTM E 1820: Standard Test Method for Measurement of Fracture Toughness. Philadelphia, 2022.
[2] American Society for Testing and Materials, ASTM E 647: Standard Test Method for Measurement of Fatigue Crack Growth Rates. Philadelphia, 2015.
[3] T.L. Anderson, Fracture mechanics, 3rd ed., Taylor & Francis Group, New York, 2005.
[4] G.A. Clarke, et al., Single specimen tests for JIC determination, in: Mechanics of Crack Growth, ASTM STP 590, Philadelphia, 1976, pp. 27–42.
[5] F.C. Moreira, G.H.B. Donato, Effects of side-grooves and 3-D geometries on compliance solutions and crack size estimations applicable to C(T), SE(B) and clamped SE(T) specimens, in: Proceedings of the ASME 2013 pressure vessels & piping division. Paris, 2013.
[6] M.A. Verstraete, et al., Evaluation and interpretation of ductile crack extension in sent specimens using unloading compliance technique, Eng. Fract. Mech. 115 (2014) 190–203.
[7] G.H.B. Donato, L.G.F. Andrade, Effects of plasticity on the elastic unloading compliance of C(T), SE(B) and Clamped SE(T) Specimens. 14th International Conference on Fracture, Rhodes, 2017.
[8] Z. Yan, W. Zhou, Effect of crack front curvature on CMOD compliance and crack length evaluation for single-edge bend specimens, in: Proceedings of the Canadian Society for Mechanical Engineering International Congress, 2014.
[9] Y. Huang, W. Zhou, Effects of crack front curvature on J-R curve testing using clamped SE(T) specimens of homogeneous materials, Int. J. Pressure Vessels Piping 134 (2015) 112–127.
[10] L.G.F. Andrade, G.H.B. Donato, M. Mattar Neto, Crack tunneling effects on the elastic unloading compliance of C(T), SE(B) and clamped SE(T) specimens and correction methodology, Theor. Appl. Fract. Mech. V (2023) 125.
[11] L.G.F. Andrade, G.H.B. Donato, Effects of crack tunneling and plasticity on the elastic unloading compliance technique for SE(B) – current limitations and proposals, Procedia Struct. Integr. v (2018) 13.
[12] G. Nikishkov, J. Heerens, D. Hellmann, Effect of crack front curvature and side grooving on CTOD δ5 and J-integral in CT and 3PB specimens, J. Test. Eval., JTEVA 27 (5) (1999) 312–319.
[13] C. Bao, L. Cai, Investigation on compliance rotation correction for compact tensile specimen in unloading compliance method, Acta Mech. Solida Sin. 24 (2) (2011).
[14] G. Shen, W.R. Tyson, Crack size evaluation using unloading compliance in single specimen single-edge-notched tension fracture toughness testing, J. Test. Eval. 37 (4) (2009).
[15] E. Wang, M. Omiya, Finite element analysis of crack mouth opening displacement compliance in crack length evaluation for clamped single edge tension specimens, Fatigue Fract. Eng. Mater. Struct. 38 (3) (2014).
[16] J. Gałkiewicz, M. Graba, Influence of the crack tip model on results of the finite elements method, J. Theor. Appl. Mech. 45 (2) (2007) 225–237.
[17] Simulia, Abaqus theory guide. [S.I.]. Abaqus Software Documentation, v.6.20, 2020.